Journal of Power Sources 226 (2013) 306–312

Contents lists available at SciVerse ScienceDirect

Journal of Power Sources

journal homepage: www.elsevier.com/locate/jpowsour

An electrocatalytic oxygen reduction by copper nanoparticles-modified Au(100)-rich polycrystalline gold electrode in 0.5 M KOH

Mohamed I. Awad [a,b], Takeo Ohsaka [a,*]

[a] Department of Electronic Chemistry, Interdisciplinary Graduate School of Science and Engineering, Tokyo Institute of Technology, 4259 Nagatsuta, Midori-ku, Yokohama 226-8502, Japan
[b] Department of Chemistry, Faculty of Science, Cairo University, Cairo, Egypt

HIGHLIGHTS

- ORR is remarkably electrocatalyzed at nano-Cu/Au$_r$ electrode.
- Catalytic activity of nano-Cu/Au$_r$ toward ORR is comparable to that of Pt.
- Enrichment of nano-Cu/Au$_r$ in Au(100) facet is behind its high catalytic activity.

ARTICLE INFO

Article history:
Received 29 August 2012
Received in revised form
22 October 2012
Accepted 7 November 2012
Available online 13 November 2012

Keywords:
Nanoparticles
Oxygen reduction
Gold
Copper
Electrocatalysis

ABSTRACT

The electrocatalytic oxygen reduction reaction (ORR) at copper nanoparticles (nano-Cu) modified Au(100)-rich polycrystalline gold electrode (nano-Cu/Au$_r$) in 0.5 M KOH is studied using cyclic and rotating disk voltammetry. The nano-Cu/Au$_r$ with a relatively enriched free Au(100) facet compared with the bare poly-Au electrode is prepared by a controlled electrodeposition of nano-Cu only on the Au(111) facet of the poly-Au electrode the other low-index facets (i.e., Au(100) and Au(110)) of which are previously covered with the self-assembled monolayer of cysteine. The electrocatalytic behavior of the nano-Cu/Au$_r$ is compared with those of the bare Au and the copper nanoparticles-modified gold electrodes (nano-Cu/Au) in which the nano-Cu is directly electrodeposited onto the poly-Au electrode. The nano-Cu/Au$_r$ shows a remarkable electrocatalysis, comparable to that of the platinum electrode, toward the ORR i.e., the ORR proceeds exclusively via a 1-step 4-electron reduction pathway at ca. 20–65 mV more positive potentials than at the bare Pt electrode, while the ORR at the nano-Cu/Au proceeds via a two-electron pathway. X-ray diffraction spectra confirms the relative enrichment of nano-Cu/Au$_r$ electrode in Au(100) facet. The relative enrichment in the free Au(100) facet of the nano-Cu/Au$_r$ electrode is thought to be behind the extraordinary electrocatalytic activity.

© 2012 Elsevier B.V. All rights reserved.

1. Introduction

Electrocatalysis for oxygen reduction reaction (ORR) is of widespread interest as it is the key subject of developing fuel cells [1–4]. Driving the ORR at low overpotential via a direct four-electron reduction is the main essential challenge in the researches on proton-exchange membrane fuel cells [5]. Several approaches have been examined to overcome the slow reaction kinetics of ORR even at the costly Pt catalyst which is of limited resources [6–10]. Among these trials, for example, alloying of Pt with some transition metals, high dispersion of Pt particles and electrodeposition of some other metals onto platinum substrate [11–15] have been extensively studied. The ORR via 2e, 4e or the combination of these two limiting cases is critically dependent on the type of catalyst as well as its crystallographic orientation and the pH of the electrolyte [16–28].

Recently nanoparticles-modified electrodes have become of great interest because of their unique electrocatalytic activities toward some electrochemical reactions as compared with their bulk counterparts [29–32]. For instance, they have been used for the catalytic hydrogenation of unsaturated alcohols and aldehydes, oxygen reduction and low temperature oxidation of CO [33–38]. The morphology and crystallographic orientation of nanoparticles can be controlled via several themes including for example the controlling of the underlying substrate–nanoparticles interactions and the co-adsorption of some additives. For example, the gold

* Corresponding author. Tel.: +81 45 924 5404; fax: +81 45 924 5489.
E-mail address: ohsaka@echem.titech.ac.jp (T. Ohsaka).

0378-7753/$ – see front matter © 2012 Elsevier B.V. All rights reserved.
http://dx.doi.org/10.1016/j.jpowsour.2012.11.010

nanoparticles prepared in the presence of iodide ion have been reported to be enriched in the Au(111) facet and those prepared in the presence of cysteine enriched in the Au(100) and Au(110) facets [39]. A critical substrate dependence of the morphology and crystallographic orientation of gold nanoparticles when deposited on Au(111), HOPG and GC substrates has been reported by our group [40]. We [41] have recently examined the electrocatalytic oxygen reduction at platinum nanoparticles (nano-Pt) modified gold electrode, in which nano-Pt was selectively electrodeposited only on the Au(111) facet of the Au electrode and subsequently the modified electrode was relatively enriched in the Au(100) facet with a higher electrocatalysis for the ORR than the Pt electrode [42], and have supposed that the peculiar morphology of the nano-Pt and the relative enrichment in the Au(100) facet of the underlying gold substrate are behind the superior catalysis for the ORR [40]. However, it remains unclear whether either or both of the two factors (i.e., the peculiar electrodeposition of nano-Pt and/or the enrichment in the Au(100) facet) cause(s) the observed superior electrocatalytic activity. To clarify this point the nano-Pt (the most active toward the ORR) used in the previous study [41] is replaced here by copper nanoparticles, which are less active than the Au electrode toward the ORR. Nano-Cu was electrodeposited either directly on the bare Au electrode or on the Au electrode modified with a submonolayer of cysteine. In the latter case the electrode was relatively enriched in the Au(100) facet, compared with the bare Au electrode. It has been reported that the Au(100) electrode is of higher catalytic activity than the Pt electrode toward the ORR in alkaline media [42–45]. The bare and modified Au electrodes were morphologically and electrochemically characterized and their electrocatalysis for the ORR in alkaline media was examined.

2. Experimental section

The polycrystalline gold (Au) and platinum (Pt) electrodes (ϕ = 1.6 mm in diameter) were polished with aqueous slurries of successively finer alumina powder (down to 0.06 μm), rinsed with water and then was sonicated for 10 min in Milli-Q water. The Au and Pt electrodes were then electrochemically pretreated in N_2-saturated 0.05 M H_2SO_4 solution by repeating the potential scan in the potential ranges of −0.2 to 1.5 V and −0.2 to 1.3 V vs. Ag/AgCl (KCl sat.), respectively, at 100 mV s^{-1} for 10 min or until the cyclic voltammograms (CVs) characteristic for clean Au and Pt electrodes were obtained.

Cu nanoparticles (nano-Cu) modified gold electrodes (nano-Cu/Au) were prepared by the electrodeposition of nano-Cu onto the bare Au electrode from 0.05 M H_2SO_4 solution containing 1 mM $CuSO_4$ by applying three consecutive potential cycles between −0.2 and 0.7 V vs. Ag/AgCl/KCl (sat.) at a scan rate of 50 mV s^{-1}. Nano-Cu/Au(100)-rich Au (nano-Cu/Au_r) was prepared by the electrodeposition of Cu onto the Au electrode modified with a submonolayer of cysteine. This was done with the aim of a preferential electrodeposition of the nano-Cu onto a specific facet domain of the Au electrode. The following strategy was employed to achieve this goal (see Scheme 1). First a full monolayer of cysteine was formed by soaking the Au electrode in aqueous solution of 1 mM cysteine. Next the cysteine was removed only from the weekly bound Au(111) facet and the Au electrode partially covered with a submonolayer of cysteine was formed (abbreviated as Au_{sm}). This was achieved by the partial reductive desorption of cysteine in 0.5 M KOH, i.e., by scanning the potential at least three times in the potential range of −0.3 to −0.8 V vs. Ag/AgCl/KCl (sat.). Then nano-Cu was electrodeposited onto the Au_{sm} in the same way as in the electrodeposition of nano-Cu on the bare Au electrode and consequently the nano-Cu/Au_{sm} was formed. The nano-Cu was electrodeposited preferentially only onto the bare Au(111) facet because

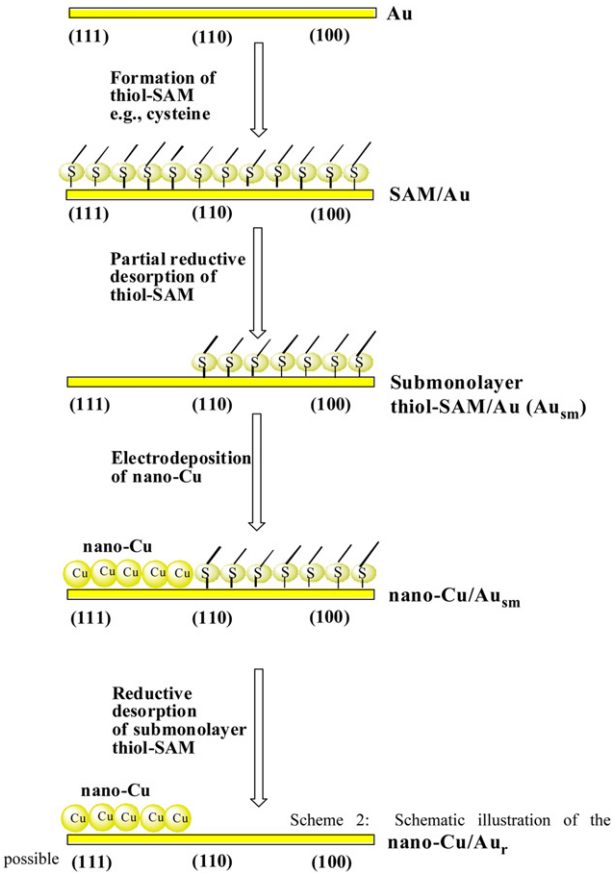

Scheme 2: Schematic illustration of the

Scheme 1. Schematic illustration of the preparation of nano-Cu/Au_r.

the other low-index facets were under the protection of cysteine (i.e., the Au(110) and Au(100) facets were covered by a cysteine monolayer). The last was the removal of the remaining cysteine on the nano-Cu/Au_{sm} by the reductive desorption in 0.5 M KOH. This was achieved by repeating the potential scan several times in the potential range between −0.3 and −1.3 V vs. Ag/AgCl (KCl sat.).

Electrochemical measurements were performed using a BAS 100 B/W electrochemical analyzer. The working electrode and the counter electrode (a platinum spiral wire) were separated by a porous glass. An Ag/AgCl (KCl sat.) electrode was used as the reference electrode. A conventional three-electrode cell of around 20 ml was used for cyclic voltammetric measurements, while in the case of hydrodynamic voltammetric measurements the working electrode compartment was 200 cm^3 to eliminate any possible change in the O_2 concentration during the measurements. Steady-state voltammograms were measured at rotating ring-disk electrode (RRDE) with Au-disk (ϕ = 6.0 mm in diameter) and Pt-ring using a rotary system from Nikko Keisoku, Japan. O_2-saturated solutions were obtained by bubbling O_2 gas for 30 min prior to each experiment and O_2 gas was flushed over the solution during the measurements.

The Au-disk-Pt-ring RRDE was mechanically polished to a mirror surface in the same manner as the Au electrode and then was cleaned ultrasonically in Milli-Q water. Then, the Au-disk of the RRDE was electrochemically treated in 10% HCl solution at 1 mA cm^{-2} for 30 min to remove any Pt contamination. After that, the RRDE was transferred into 0.1 M H_2SO_4 solution and hydrogen gas was evolved at both electrodes for removing any adsorbed chloride [46]. The collection efficiency, N, of the RRDE was measured using 1.0 mM $K_3[Fe(CN)_6]$ in 0.5 M KCl, and a value of

0.42 ± 0.02 was obtained. Electrolyte solutions were, if necessary, deaerated by bubbling N_2 gas for at least 30 min prior to electrochemical measurements. All the measurements were performed at room temperature (25 ± 1 °C). All the current densities were calculated on the basis of the geometric surface area of the relevant working electrode.

X-ray diffraction (XRD) measurements were performed on a Philips PW 1700 powder X-ray diffractometer using Cu $K_{\alpha 1}$ radiation ($\lambda = 1.54056$ Å) with a Ni filter working at 40 kV and 30 mA. Scanning electron microscopy (SEM) and electron diffraction spectroscopy (EDS) analysis of the bare and modified Au electrodes was carried out using an JSM-T220 scanning electron microscope (JEOL Optical Laboratory, Japan) at an acceleration voltage of 20 kV and a working distance of 4–5 mm.

3. Results and discussion

3.1. Morphological characterization

Fig. 1 shows SEM images of (a) nano-Cu/Au and (b) nano-Cu/Au_r electrodes. The image of the nano-Cu/Au_r electrode shows the deposition of copper nanoparticles of ca. 30–50 nm in size, while a deposition of copper particles with a relatively larger size of ca. 200 nm is observed for the nano-Cu/Au. The relatively uniform electrodeposition of Cu in the case of the nano-Cu/Au_r electrode may be attributed to the controlled deposition of Cu, i.e., it is thought that Cu may be deposited possibly on the bare fraction of the underlying Au electrode (i.e., Au(111) facet), underneath the cysteine SAM (i.e., on the Au(100) and Au(110) facets) and atop the cysteine SAM. In the present case, the second possibility is excluded because the deposition is conducted for a short time and thus there seems to be no chance for the deposition to occur underneath the cysteine SAM. The third possibility is also excluded because the charge transfer on the bare fraction of the underlying Au electrode is much easier than through the cysteine SAM [41,47,48]. Thus it is believed that the Cu is deposited favorably on the Au(111) facet. It has been reported that the deposition of Cu on SAM modified electrodes can take place through the defects, i.e., on the underlying electrode and for this reason it has been used as a defect marker of the SAM [3,49–53].

Fig. 2 shows the EDS spectra of bare and nano-Cu modified Au electrodes. In the case of nano-Cu/Au (spectrum b) and nano-Cu/Au_r (spectrum c) the peak of copper is shown at energy around 0.75 eV. The peak intensity of copper at the former is feasible, while the one at the latter electrode is not revealed. This indicates that the deposition of copper in the case of nano-Cu/Au is larger than that at nano-Cu/Au_r consistently with SEM results shown above. This might be due to the controlled electrodeposition of copper in the case of nano-Cu/Au_r which leads to a sparse deposition of nano-Cu.

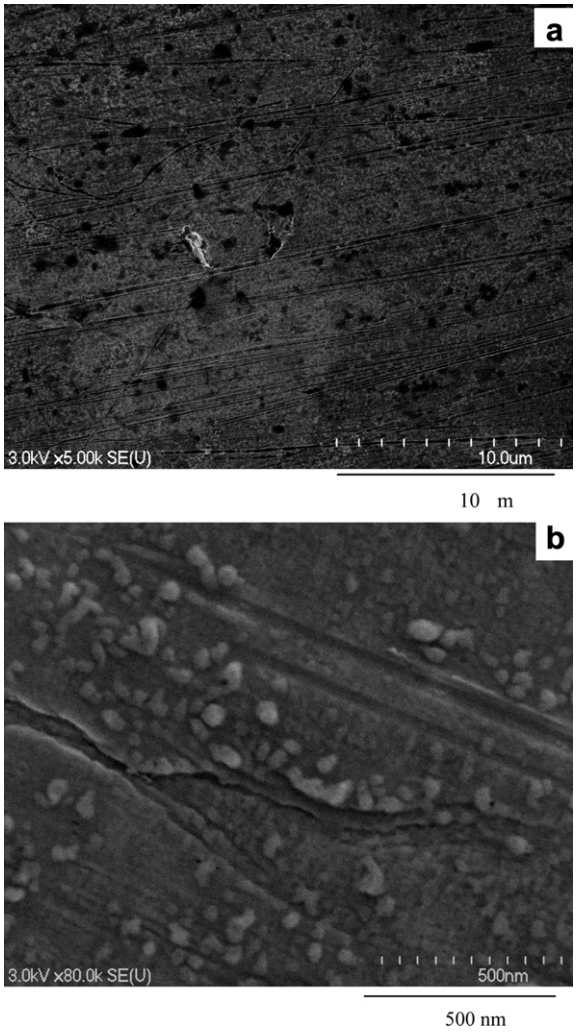

Fig. 1. SEM images obtained at (a) nano-Cu/Au and (b) nano-Cu/Au_r electrodes.

3.2. Electrochemical characterization

Fig. 3 shows CVs obtained at (a) bare Au, (b) nano-Cu/Au and (c) nano-Cu/Au_r electrodes in N_2-saturated 0.5 M KOH. The characteristic CV of a clean Au electrode is clearly shown in curve (a) in which the oxidation peak (at ca. 0.2–0.8 V) that corresponds to the formation of gold oxide is coupled with the reduction one centered at ca. 0.07 V. The oxidation peak is preceded by the formation of an oxide precursor in a wide potential region, from −0.3 V to 0.2 V. This precursor formation represents the partial charge transfer in the adsorption of hydroxide. The oxidation peak extending over a wide range of potential reflects the oxidation of the different facets of the Au electrode, i.e., Au(111), Au(110) and Au(100). The reduction peak current at ca. 0.07 V is smaller at the nano-Cu/Au_r electrode (curve c) than at the nano-Cu/Au electrode (curve b). In addition the appearance of a new couple ($E_{½} = -0.125$ V vs. Ag/AgCl) confirms the electrodeposition of copper [54]. This

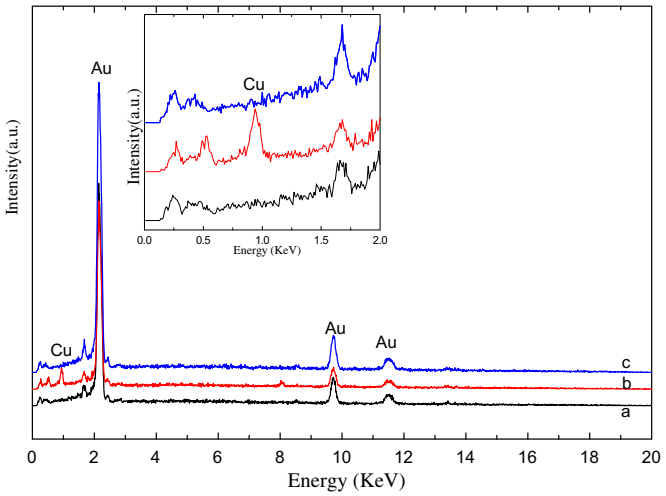

Fig. 2. EDS spectra for the (a) bare Au, (b) nano-Cu/Au and (c) nano-Cu/Au_r electrodes. Inset shows the enlargement at low energy.

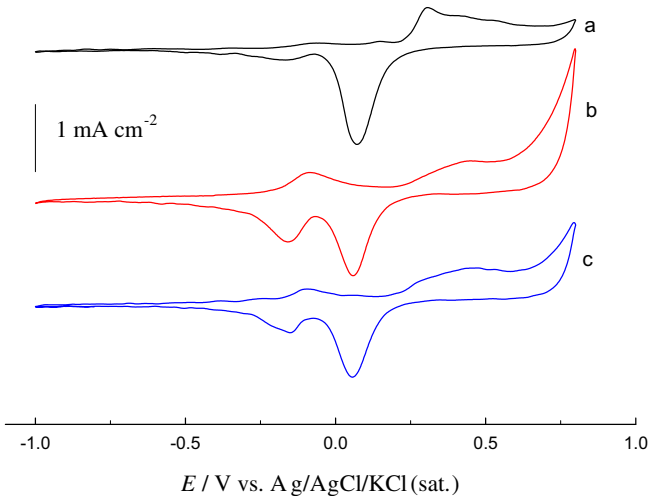

Fig. 3. CVs obtained at (a) bare Au, (b) nano-Cu/Au and (c) nano-Cu/Au$_r$ electrodes in N_2-saturated 0.5 M KOH. Potential scan rate: 100 mV s^{-1}.

consistently agrees with the SEM and EDS results shown above which indicate that the fraction of the underlying Au electrode covered with the nano-Cu is larger at the nano-Cu/Au$_r$ electrode than at the nano-Cu/Au electrode. Interestingly the oxidation peak (ca. 0.2–0.8 V), which corresponds to the oxidation of the different facets, shows different shapes at the individual electrodes. This reflects the different crystallographic orientation of the uncovered facets of the underlying Au electrode. However, it is difficult to quantify the ratios of the different facets of the individual underlying substrates.

Shown in Fig. 4 are the CVs obtained for the ORR at (a) bare Au, (b) nano-Cu/Au, (c) nano-Cu/Au$_r$ and (d) bare Pt electrodes in O_2-saturated 0.5 M KOH. A typical linear scan voltammetry profile controlled by the diffusion is obtained. First O_2 is reduced to hydrogen peroxide (HO_2^- in alkaline media) at ca. −167 mV and further it is reduced to water (OH^- in alkaline media) at

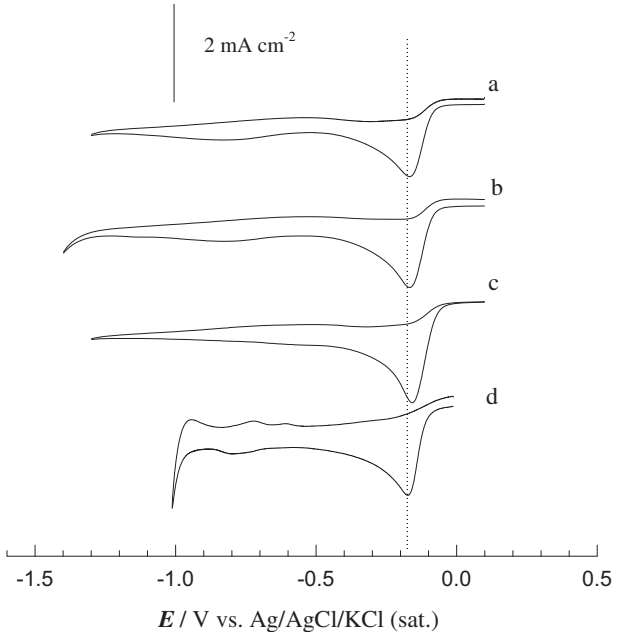

Fig. 4. CVs obtained for the ORR at (a) bare Au, (b) nano-Cu/Au, (c) nano-Cu/Au$_r$ and (d) bare Pt electrodes in O_2-saturated 0.5 M KOH. Potential scan rate: 100 mV s^{-1}.

ca. −810 mV. The nano-Cu/Au shows the similar behavior (curve b) to the Au electrode (curve a). The main difference is a slight increase in the first reduction peak current together with a slight decrease in the second one. The nano-Cu/Au$_r$ electrode, interestingly, shows only one peak at around −150 mV (curve c), the current of which is almost twice the first peak current at the Au electrode and is comparable to that obtained at the Pt electrode (curve d). This indicates that the ORR occurs via a one-step 4-electron pathway at the nano-Cu/Au$_r$ electrode. This fact could be explained by considering the relative enrichment of Au(100) facet in the underlying Au substrate (in the case of the nano-Cu/Au$_r$) as a result of the preferential electrodeposition of nano-Cu onto the bare fraction of the Au$_{sm}$ electrode (i.e., Au(111) domain) as mentioned above. Here the role of nano-Cu is to cover the least active Au(111) facet for the ORR, resulting in the relative enrichment of the other two low-index facets (i.e., Au(110) and Au(100)). It is thought that the high electrocatalytic activity of the nano-Cu/Au$_r$ electrode for the ORR is due to the relative enrichment of the Au(100) facet, but not due to the electrodeposited nano-Cu, because in alkaline media O_2 is reduced on Cu electrode at much more negative potentials compared with the Au electrode [55]. Also from Fig. 4, we can see that the cathodic peak potential for the ORR at the nano-Cu/Au$_r$ electrode is more positive than those at the bare Au and nano-Cu/Au electrodes as well as the Pt electrode (curve d), as expected from the fact that the Au(100) electrode possesses a higher electrocatalysis for the ORR than the Pt electrode in alkaline media [42].

Fig. 5 shows the disk (lower panel) current for the ORR at (a) bare Au, (b) bare Pt, (c) nano-Cu/Au and (d) nano-Cu/Au$_r$ disk

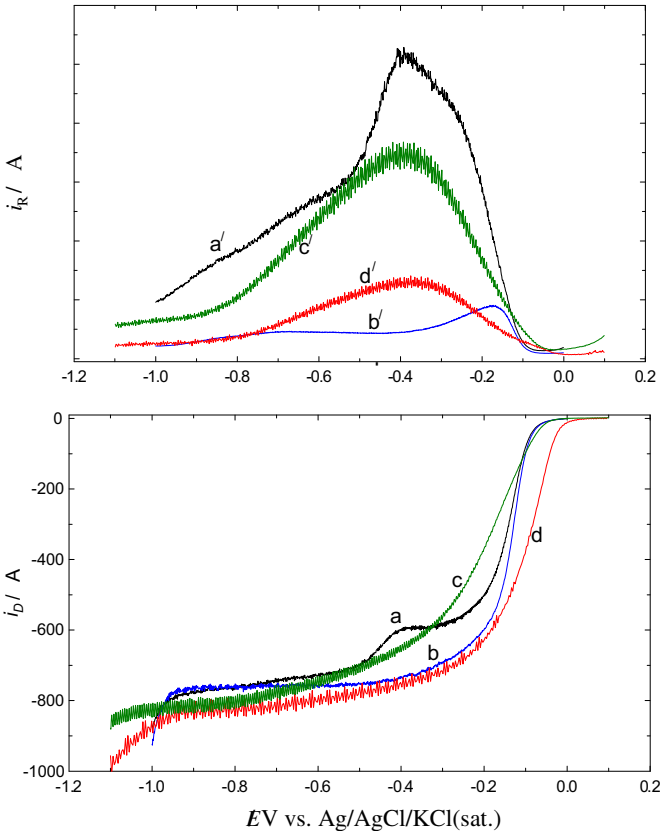

Fig. 5. Steady-state voltammograms for the ORR at (a) bare Au, (b) bare Pt, (c) nano-Cu/Au and (d) nano-Cu/Au$_r$ disk electrodes and the corresponding HO_2^- oxidation at (a′, b′, c′ and d′) Pt-ring electrode in O_2-saturated 0.5 M KOH solution. The Pt-ring was potentiostated at 500 mV vs. Ag/AgCl (KCl sat.). Rotation rate: 800 rpm. Potential scan rate: 10 mV s^{-1}. (Note that the geometric surface area of each disk electrode is 0.28 cm^{-2}).

electrodes and the corresponding ring (upper panel) current (for HO_2^- oxidation) at (a′, b′, c′ and d′) Pt-ring electrode in O_2-saturated 0.5 M KOH solution. At the Au-disk electrode (curve a) two limiting current regions are obtained indicating the 2-step 4-electron reduction of O_2 via hydrogen peroxide HO_2^- (as an intermediate) to OH^-. The ring current increases (curve a′) upon scanning the Au-disk potential to the negative direction (curve a) indicating the predominance of the 2-electron reduction of O_2 to HO_2^-, and then further reduction of HO_2^- to OH^- occurs as can be seen from the gradual decrease in the ring current at more negative disk potential. As expected, only one limiting current region is obtained at the bare Pt disk electrode (curve b), which is accompanied by significantly small ring current indicating the exclusive 4-electron reduction of O_2 to OH^-. In the case of the nano-Cu/Au-disk electrode (curve c) almost similar behavior to that at the bare Au electrode is obtained. However, in this case, consistently with the results shown in Fig. 4, the ring current is smaller than at the Au electrode. On the other hand, at the nano-Cu/Au$_r$ disk electrode, interestingly, the contribution of the 2-electron reduction of O_2 to HO_2^- is much smaller than that obtained at the bare Au and nano-Cu/Au electrodes as being obvious from the lower ring current. Furthermore, the reduction wave is totally shifted to the positive direction of potential and the limiting current is achieved at relatively positive potential, as compared with those obtained at the bare Pt electrode.

Among the mechanisms reported for ORR the one shown in Scheme 2 is reported to be suitable for Pt-group metals [56]. ORR mechanism, whether it is 1-step 4-electron reduction or 2-step 4-electron reduction, is inherently related to the nature of the electrode. It is also, in some cases, critically dependent on the crystallographic orientation of the electrode surface. For instance, the Au(100) electrode supports a direct 4-electron reduction of molecular oxygen (Eq. (1)) at potentials fairly positive to that obtained at the poly-Pt electrode in alkaline media [42]. Whereas the Au(111) single crystalline electrode shows the least activity toward the same reaction as it supports a quasi-reversible 2-electron reduction pathway [43]. Thus, at poly-Au electrode, both 2-step 4-electron reduction (stepwise mechanism, Eqs. (2) and (3)) and 1-step 4-electron reduction may take place.

$$O_2 + 2H_2O + 4e = 4OH^- \quad (1)$$

$$O_2 + H_2O + 2e = HO_2^- + OH^- \quad (2)$$

$$HO_2^- + H_2O + 2e = 4OH^- \quad (3)$$

The mechanism of oxygen reduction could be quantitatively probed by considering the relative ratio of the ring current (i_R) to the disk current (i_D), which is correlated with the total number of electrons (n) exchanged during the reduction of one oxygen molecule by [56]

$$n = \frac{4i_D}{\left(i_D + \left(\frac{i_R}{N}\right)\right)} \quad (4)$$

where

$$Ni_D/iR = 1 + 2k_1/k_2 + A + \left(k_6 A/Zw^{1/2}\right) \quad (5)$$

with

$$A = (2k_1/k_2k_5)(k_{-2} + k_3 + k_4) + (2k_3 + k_4)/k_5 \quad (6)$$

where N is the collection efficiency of the RRDE electrode (in this case 0.42 ± 0.02), w is the rotation rate, and $Z = 0.62D^{2/3}\,\nu^{-1/6}$ [D is the diffusion coefficient of O_2 and ν is the kinematic viscosity of the solution]. The rate constant k_i pertains to the i-th reaction according to the following notation: (1) 4-electron direct reduction of O_2 to OH^-, (2) 2-electron reduction of $O_{2(a)}$ to $HO_{2(a)}^-$, (−2) oxidation of $HO_{2(a)}^-$ to $O_{2(a)}$, (3) 2-electron reduction of $HO_{2(a)}^-$ to OH^-, (4) catalytic decomposition of $HO_{2(a)}^-$ to $O_{2(a)}$ and OH^-, (5) desorption of $HO_{2(a)}^-$ and (6) adsorption of HO_2^{-*}. A value of 2 for n, obtained when $i_R/Ni_D = 1$, indicates the predominance of the hydrogen peroxide path, i.e., 1-step 2-electron reduction, i.e., $k_1 = 0$ and $(2k_3 + k_4)$ is close to zero, while a value of $n = 4$, obtained when $i_R/Ni_D = 0$, means a negligible contribution of the hydrogen peroxide formation pathway, i.e., $k_2 = 0$, i.e., the exclusive direct reduction of O_2 to OH^-. The relative ratio of the 2-electron to the 4-electron reduction pathway of O_2 to HO_2^- and OH^- is governed by the stability of the adsorbed intermediate (i.e., $HO_{2(a)}^-$) on the electrode surface. As can be seen from the ring current in Fig. 5, the production of hydrogen peroxide is largely decreased at the nano-Cu/Au$_r$ electrode compared with the poly-Au electrode. This means that the 4-electron reduction of O_2 to OH^- becomes dominant at the former electrode as a result of the relative enrichment of Au(100) facet. In other words, the more O_2 molecules, which diffuse to the electrode surface, undergo 4-electron reduction at the nano-Cu/Au$_r$ electrode with a relatively enriched Au(100) facet compared with the poly-Au electrode and at the poly-Au electrode with Au(111) facet a part of O_2 molecules diffusing to the electrode surface undergo 2-electron reduction on this facet to form hydrogen peroxide.

Fig. 6 shows the dependence of n on the potential at the Au (curve a), Pt (curve b), nano-Cu/Au (curve c) and nano-Cu/Au$_r$ (curve d) disk electrodes. At the bare Au-disk (curve a) and nano-Cu/Au electrodes, the n decreases as the disk potential is scanned to the negative direction of potential, reaches a minimum at ca. −0.4 V which is much larger than 2 and then gradually increases at more negative potentials. This indicates that at potentials more positive than ca. −0.4 V O_2 is reduced to HO_2^- which partially disproportionates into molecular oxygen and water at the Au-disk electrode (Eq. (7)) and further reduction of HO_2^- to OH^- takes place at potentials more negative than ca. −0.4 V.

$$2HO_2^- = O_2 + 2OH^- \quad (7)$$

On the other hand, at the nano-Cu/Au$_r$ disk electrode the values of n are much larger than those at the bare Au and nano-Cu/Au electrodes and are almost close to 4 in a wide potential range of −0.05 to −1.1 V except for the potential range of ca. −0.3 to −0.6 V in which the n is ca. 3.7–3.9 (curve d) indicating that O_2 is exclusively reduced via a 1-step 4-electron reduction to OH^-. A negligible contribution of the 2-electron reduction is more significantly observed at the nano-Cu/Au$_r$ compared to the nano-Cu/Au.

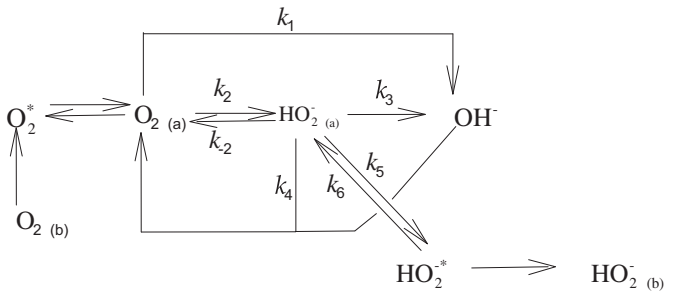

Scheme 2. Schematic illustration of the possible reduction pathways of O_2 in alkaline media. The subscripts (a) and (b) refer to adsorbed state and bulk solution species, respectively. The superscript (*) refers to the electrode-vicinity species. The k's are the rate constant of the relevant steps.

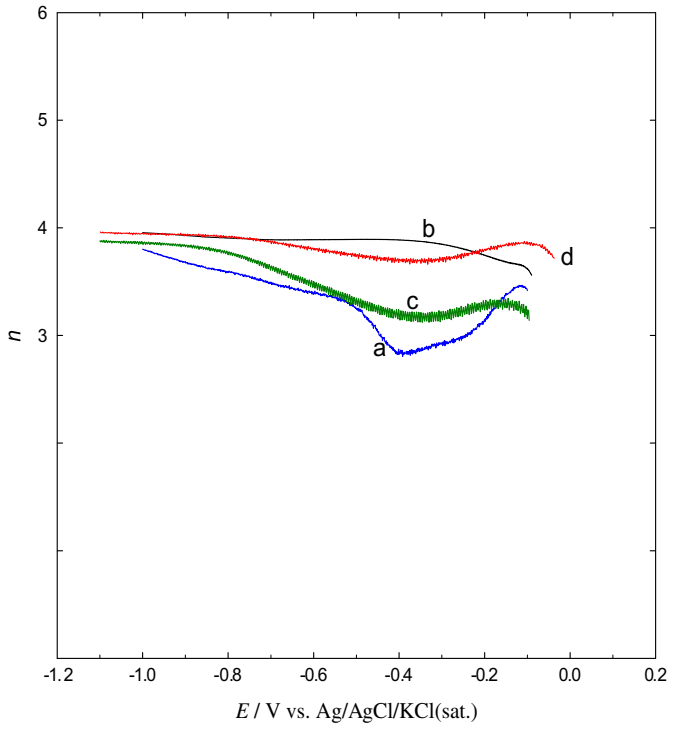

Fig. 6. Dependence of n on the disk electrode potential for the ORR in O_2-saturated 0.5 M KOH at (a) bare Au, (b) bare Pt, (c) nano-Cu/Au and (d) nano-Cu/Au_r electrodes. The data were extracted from Fig. 5.

In addition, it is obvious that in the potential range of 0 to −0.2 V (i.e., at the rising part of the voltammogram) the values of n at the nano-Cu/Au_r electrode are larger than those at the Pt electrode, i.e., close to 4.

To investigate the reason behind the high catalytic activity obtained at the nano-Cu/Au_r electrode, the three electrodes, i.e., bare Au, nano-Cu/Au and nano-Cu/Au_r electrodes were dipped in 1 mM cysteine aqueous solution for enough time to form a self-assembled monolayer (SAM) of cysteine on the individual electrodes. Then, the reductive desorption of the cysteine SAM was carried out in N_2-saturated 0.5 M KOH and the results are shown in Fig. 7. Thiols are characterized by their spontaneous adsorption on Au electrode forming a monolayer via the formation of Au–S bond. The strength of this bond is dependent on the crystallographic orientation of the gold substrate in the following order; S–Au(100) > S–Au(110) ≫ S–Au(111) [56,57]. Thus, the reductive desorption pattern for cysteine from the Au electrode is characterized by three reduction peaks the potentials of which can be correlated to the Au–S bond strength, i.e., the cysteine SAM with a stronger Au–S bond is desorbed at more negative potential. The reductive desorption of cysteine from the Au electrode shows three reduction peaks at −0.69, −1.0 and ca. −1.1 V (voltammogram a), which correspond to the desorption of cysteine from Au(111), Au(110) and Au(100) facets, respectively [43,57].

Similar behavior was observed for the reductive desorption of cysteine from the nano-Cu/Au electrode (voltammogram b). However, in this case, the third peak is overlapped with the enhanced hydrogen evolution due to the deposited Cu nanoparticles. In alkaline media the exchange current density of the hydrogen evolution reaction at the Cu electrode is by one order of magnitude larger than that at the Au electrode [58]. Interestingly, in the case of the nano-Cu/Au_r electrode (voltammogram c), the peak at 0.69 V which corresponds to the desorption of cysteine from the Au(111) facet could not be observed at all. This confirms a significant coverage of the Au(111) facet by the deposited nano-Cu, resulting in the relative enrichment of the Au(100) facet, that is, the high electrocatalytic activity of the nano-Cu/Au_r electrode toward the ORR in alkaline media compared with the Au and nano-Cu/Au electrodes.

For further insight into the reason behind the catalytic activity of nano-Cu/Au_r electrode toward oxygen reduction the XRD spectra of the three studied electrodes, i.e., (a) bare Au, (b) nano-Cu/Au and (c) nano-Cu/Au_r, were taken and are shown in Fig. 8. Inset shows the enlargement in the range which shows the peak of Au(111) facet. The diffraction peaks obtained at the bare Au electrode at 2θ of ca. 38.2 and 44.4° correspond to the Au(111) and Au(200) facets, respectively [59] (spectrum a). These two peaks are also observed in the spectra of nano-Cu/Au and nano-Cu/Au_r electrodes, together with two small peaks at 64.5 and 77.7° which correspond to the (220) and (331) facets, respectively. The interesting point is that the diffraction intensity ratios of the two peaks corresponding to the Au(111) and Au(200) facets are significantly different at the three examined electrodes: At the nano-Cu/Au electrode the diffraction intensity of the Au(111) facet largely increases, but that of the Au(200) facet decreases, compared with the bare Au electrode. On the other hand, at the nano-Cu/Au_r electrode, the Au(200) facet

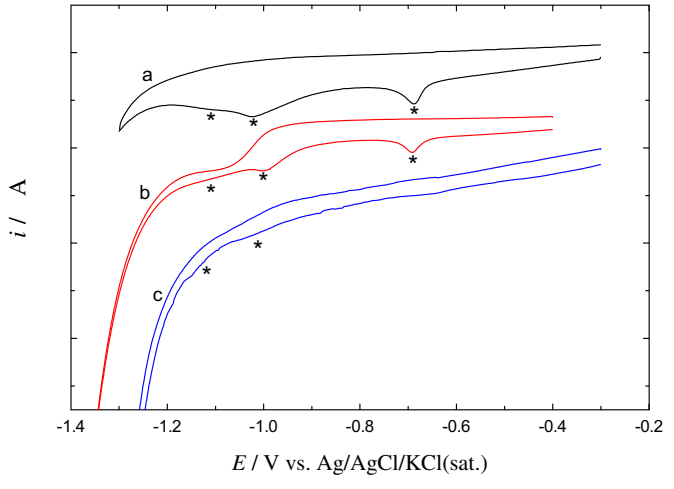

Fig. 7. CVs for the reductive desorption of the cysteine SAM assembled onto the (a) bare Au, (b) nano-Cu/Au and (c) nano-Cu/Au_r electrodes in N_2-saturated 0.5 M KOH. Potential scan rate: 50 mV s^{-1}.

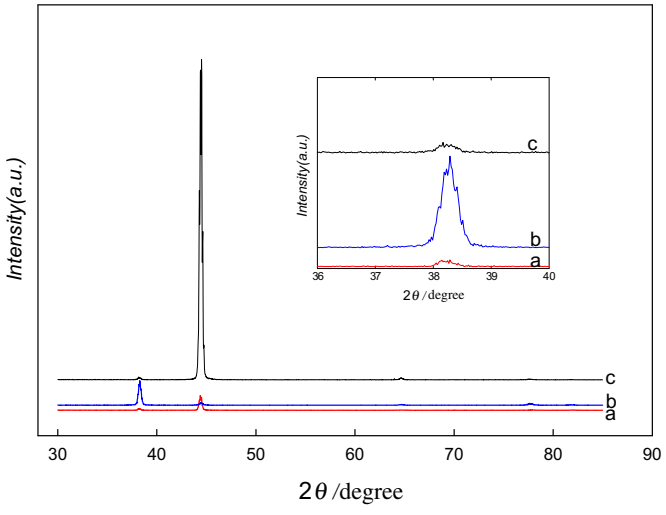

Fig. 8. XRD spectra for the (a) bare Au, (b) nano-Cu/Au and (c) nano-Cu/Au_r electrodes. Inset shows the enlargement in the range of Au(111) facet.

diffraction intensity significantly increases compared with that obtained at the bare Au electrode. Here, it is worthy of remark that according to the extinction rule the (200) facet is equivalent to the Au(100) facet [60]. Thus, we can say that the selective deposition of Cu on the Au polycrystalline electrode employed in the fabrication of the nano-Cu/Au$_r$ electrode, in which the Au(100) and Au(110) facets are selectively covered by cysteine and the Cu is electrodeposited only on the uncovered Au(111) facet and then the cysteine on the Au(100) and Au(110) facets are removed by the reductive desorption, results in the "ORR-active" Au electrode which is relatively enriched in Au(100) facet. Au(100) facet is the most active low-index facet of the Au electrode for the ORR and supports a direct 4-electron reduction of O_2 to OH^- [26,42,61]. This high catalytic activity may be attributed to the enhanced dissociative adsorption of HO_2^- anions on the 4-fold symmetric sites which occurs only on the Au(100) facet [42]. Thus it can be concluded that the relative enrichment of the nano-Cu/Au$_r$ electrode in the Au(100) facet or the complete coverage (by ORR-inactive nano-Cu) of the least active facet for the ORR (i.e., Au(111)) is behind the observed high electrocatalysis of the nano-Cu/Au$_r$ electrode toward the ORR in alkaline media.

4. Conclusions

A novel non-platinum electrocatalyst (nano-Cu/Au$_r$) supporting a direct 4-electron reduction pathway for the ORR at a relatively less negative potential compared with the Pt electrode was proposed. This catalyst was prepared by the controlled electrodeposition of nano-Cu on the Au electrode modified with a submonolayer of cysteine: The electrodeposition of nano-Cu was forced to occur on the bare fraction of the Au (i.e., Au(111) facet), while the other low-index facets (i.e., Au(110) and Au(100)) were under the protection of the cysteine submonolayer, and then the submonolayer of cysteine was completely removed by the reductive desorption in 0.5 M KOH solution. The observed high electrocatalytic activity is due to the relative enrichment in the free Au(100) facet of the nano-Cu/Au$_r$ electrode on which the ORR proceeds via a 4e-reduction process in alkaline media.

Acknowledgments

The present work was financially supported by Grant-in-Aid for Scientific Research (A) (No. 19206079) from the Ministry of Education, Culture, Sports, Science and Technology (MEXT), Japan and New Energy and Industrial Technology Development Organization (NEDO), Japan.

References

[1] N.M. Markovic, H.A. Gasteiger, P.N. Ross, J. Phys. Chem. 16 (1996) 6715.
[2] A. Damjanovic, D.B. Sepa, Electrochim. Acta 35 (1990) 1157.
[3] M. Nishizawa, T. Sunagawa, H. Yoneyama, Langmuir 13 (1997) 5215.
[4] R. Adzic, in: J. Lipkowski, P.N. Ross (Eds.), Electrocatalysis, Wiley-VCH, New York, 1998, pp. 197–242.
[5] H.A. Gasteiger, S.S. Kocha, B. Sompalli, F.T. Wagner, Appl. Catal. B 56 (2005) 9.
[6] E. Higuchi, H. Uchida, M. Watanabe, J. Electroanal. Chem. 583 (2005) 69.
[7] R. Jiang, D. Chu, J. Electrochem. Soc. 147 (2000) 4605.
[8] R. Halseid, M. Heinen, Z. Jusys, R.J. Behm, J. Power Sourc. 176 (2008) 435.
[9] G. Lalande, R. Cote, D. Guay, J.P. Dodelet, L.T. Weng, P. Bertrand, Electrochim. Acta 42 (1997) 1379.
[10] M. Lefevre, J.P. Dodelet, P. Bertrand, J. Phys. Chem. B 104 (2000) 11238.
[11] J. Zhang, M.B. Vukmirovic, K. Sasaki, A.U. Nilekar, M. Mavrikakis, R.R. Adzic, J. Am. Chem. Soc. 127 (2005) 12480.
[12] J. Zhang, M.B. Vukmirovic, Y. Xu, M. Mavrikakis, R.R. Adzic, Angew. Chem. Int. Ed. 44 (2005) 2132.
[13] S. Koh, P. Strasser, J. Am. Chem. Soc. 129 (2007) 12624.
[14] V.R. Stamenkovic, B. Fowler, B.S. Mun, G.F. Wang, P.N. Ross, C.A. Lucas, N.M. Markovic, Science 315 (2007) 493.
[15] F.H. Lima, J.F. de Castro, L.G. Santos, E.A. Ticianelli, J. Power Sourc. 190 (2009) 293.
[16] J. Perez, H.M. Villullas, E.R. Gonzalez, J. Electroanal. Chem. 435 (1997) 179.
[17] Y.J. Li, C.C. Chang, T.C. Wen, J. Appl. Electrochem. 27 (1997) 227.
[18] C.C. Chang, T.C. Wen, Mater. Chem. Phys. 47 (1997) 203.
[19] C.C. Chang, T.C. Wen, H.J. Tien, Electrochim. Acta 42 (1997) 557.
[20] A.J. Damjanovic, J. Electrochem. Soc. 138 (1991) 2315.
[21] C.C. Chang, T.C. Wen, J. Electrochem. Soc. 143 (1996) 1485.
[22] J. Prakash, H. Joachin, Electrochim. Acta 45 (2000) 2289.
[23] R.R. Adzic, J. Zhang, K. Sasaki, M.B. Vukmirovic, M. Shao, J.X. Wang, A.U. Nilekar, M. Mavrikakis, J.A. Valerio, F. Uribe, Top. Catal. 46 (2007) 249.
[24] J. Zhang, Y. Mo, M.B. Vukmirovic, R. Klie, K. Sasaki, R.R. Adzic, J. Phys. Chem. B 108 (2004) 10955.
[25] R.R. Adzic, N.M. Markovic, V.B. Vesovie, J. Electroanal. Chem. 165 (1984) 105.
[26] R.R. Adzic, N.M. Markovic, V.B. Vesovie, J. Electroanal. Chem. 165 (1984) 121.
[27] J. Kim, A.A. Gewirth, J. Phys. Chem. B 110 (2006) 2565.
[28] J. Zhang, F.H. Lima, M.H. Shao, K. Sasaki, J.X. Wang, J. Hanson, R.R. Adzic, J. Phys. Chem. B 109 (2005) 22701.
[29] S.H. Joo, K. Kwon, D.J. You, C. Pak, H. Chang, J.M. Kim, Electrochim. Acta 54 (2009) 5746.
[30] I. Roche, E. Chaine, M. Chatenet, J. Vondrak, J. Phys. Chem. C 111 (2007) 1434.
[31] M.L. Calegar, F.H. Lima, E.A. Ticianelli, J. Power Sourc. 158 (2006) 735.
[32] W. Yao, J. Yang, J. Wang, Y. Nuli, Electrochem. Commun. 9 (2007) 1029.
[33] M.S. El-Deab, T. Ohsaka, Electrochem. Commun. 4 (2002) 288.
[34] M.S. El-Deab, T. Ohsaka, Electrochim. Acta 47 (2002) 4255.
[35] S. Schimpf, M. Lucas, C. Mohr, U. Rodemerck, A. Bruckner, J. Radnik, H. Hofmeister, P. Claus, Catal. Today 72 (2002) 63.
[36] M. Haruta, Catal. Today 36 (1997) 153.
[37] A.D. Sarkar, B.C. Khanra, J. Mol. Catal. A Chem. 229 (2005) 25.
[38] M. Haruta, M. Date, Appl. Catal. A Gen. 222 (2001) 427.
[39] M.S. El-Deab, T. Sotomura, T. Ohsaka, J. Electrochem. Soc. 152 (2005) C1.
[40] M.S. El-Deab, T. Sotomura, T. Ohsaka, J. Electrochem. Soc. 152 (2005) C730.
[41] M.I. Awad, M.S. El-Deab, T. Ohsaka, J. Electrochem. Soc. 154 (2007) B810.
[42] N.M. Markovic, I.M. Tidewell, P.N. Ross, Langmuir 10 (1994) 1.
[43] M.S. El-Deab, K. Arihara, T. Ohsaka, J. Electrochem. Soc. 151 (2004) E213.
[44] S. Strbac, R. Adzic, Electrochim. Acta 41 (1996) 2903.
[45] C. Paliteiro, N. Martins, Electrochim. Acta 44 (1998) 1359.
[46] J. Maruyama, M. Inaba, Z. Ogumi, J. Electroanal. Chem. 458 (1998) 175.
[47] S. Kuwabata, H. Kanemoto, D. Oyamatsu, H. Yoneyama, Electrochemistry 67 (1999) 1254.
[48] H. Hagenstrom, M.J. Esplandiu, D.M. Kolb, Langmuir 17 (2001) 839.
[49] G.M. Whitesides, Langmuir 6 (1990) 87.
[50] L. Sun, R.M. Crooks, J. Electrochem. Soc. 138 (1991) L23.
[51] J.A. Sondag-Huetinst, Langmuir 11 (1995) 4823.
[52] G.K. Jennings, P.E. Laibinis, Langmuir 12 (1996) 6173.
[53] C.M. Whelan, M.R. Smyth, C.J. Barnes, Langmuir 15 (1999) 116.
[54] H. Mohammadi, A. Amine, M. El Rhazi, C.M.A. Brett, Talanta 62 (2004) 951–958.
[55] K. Balakrishnan, V.K. Venkatesan, Electrochim. Acta 24 (1979) 131.
[56] H.S. Wrobiowa, Y. Pan, G. Razumney, J. Electroanal. Chem. 69 (1976) 195.
[57] K. Arihara, T. Ariga, N. Takashima, K. Arihara, T. Okajima, F. Kitamura, K. Tokuda, T. Ohsaka, Phys. Chem. Chem. Phys. 5 (2003) 3728.
[58] T. Valand, Int. J. Hydrogen Energy 22 (1997) 669.
[59] T. Kinoshita, S. Seino, K. Okitsu, T. Nakayama, T. Nakagawa, T.A. Yamamoto, J. Alloys Compd. 359 (2003) 46.
[60] T. Izumi, I. Watanabe, Y. Yokoyama, J. Electroanal. Chem. 303 (1991) 151.
[61] N.M. Markovic, R.R. Adzic, V.B. Veaovic, J. Electroanal. Chem. 165 (1981) 106.